CRACKNELL, A. P. (1972). *Acta Cryst.* A**28**, 597-601.
CRACKNELL, A. P. (1975). *Magnetism in Crystalline Materials. Applications of the Theory of Groups of Cambient Symmetry.* Oxford: Pergamon Press.
KOPSKY, V. (1976). *J. Magn. Magn. Mater.* **3**, 201-211.
NERONOVA, N. N. & BELOV, N. V. (1960). *Sov. Phys. Crystallogr.* **4**, 769-774.
OPECHOWSKI, W. (1985). *Crystallographic and Metacrystallographic Groups.* Amsterdam: North Holland.
OPECHOWSKI, W. & GUCCIONE, R. (1965). *Magnetism*, Vol. IIA edited by G. T. Rado & H. Suhl, pp. 105-165 New York: Academic Press.
SCHWARZENBERGER, R. L. E. (1984). *Bull. London Math. Soc.* **16**, 209-240.

*Acta Cryst.* (1986). A**42**, 47-55

# Neutron Diffraction Investigation of the Nuclear and Magnetic Extinction in MnP

BY J. BARUCHEL

*Institut Laue-Langevin*, 156*X*, 38042 *Grenoble CEDEX, France*

C. PATTERSON

*Department of Applied Physics, University of Hull, Hull HU6 7RX, England*

AND J. P. GUIGAY

*Laboratoire Louis Néel, CNRS-USMG*, 166*X*, 38042 *Grenoble CEDEX, France*

(*Received* 8 *May* 1985; *accepted* 22 *August* 1985)

## Abstract

The absolute values of the reflecting powers $\rho$ are measured for the 200 and $2 \pm \tau,0,0$ set of magnetic and nuclear reflections in the helimagnetic phase of a good-quality crystal of MnP as a function of its thickness. Severe and very different extinction effects are observed for the magnetic and nuclear reflections ($y_{\text{magnetic}} \sim 0{\cdot}4$, $y_{\text{nuclear}} \sim 0{\cdot}02$ for the largest thickness). This corresponds to the spectacular result that the magnetic reflecting powers $\rho_{\pm}$ are twice as big as the nuclear one $\rho_N$, in spite of the fact that the scattering cross sections $|F_{\pm}|^2$ are about ten times smaller than the nuclear $|F_N|^2$. The nuclear results appear consistent with dynamical theory while the magnetic ones are not. They can be explained by Zachariasen's type II secondary extinction model based on the chirality domain pattern. The same measurements were performed in the ferromagnetic phase, yielding $y_{\text{ferro}} \simeq 0{\cdot}03$. A model using the relative sizes of the ferromagnetic and chirality domains is presented.

## I. Introduction

The basic publication on extinction for the neutron case, within the framework of the mosaic model, is now nearly forty years old (Bacon & Lowde, 1948). Since then most of the improvements introduced to correct the extinction of the intensities diffracted by a single-crystal sample originate from the theory based on the Darwin energy transfer equations worked out by Zachariasen (1967). This theory was modified to take into account the anisotropy of the extinction by Coppens & Hamilton (1970) and Thornley & Nelmes (1974). The formalism was reconsidered and improved by Cooper & Rouse (1970) and Becker & Coppens (1974*a*, *b*) in order to apply it to spherical or ellipsoidal crystals, the theory being extended to non-spherical crystals with anisotropic extinction by Becker & Coppens (1975).

The main limitation of Zachariasen's theory is in its kinematical approach to the scattering, as pointed out by Werner (1969, 1974): the coherence of the transmitted and diffracted beams is not taken into account, and so this method does not appear to be suitable for correction for severe primary extinction. Another approach, starting from the dynamical theory of diffraction, was worked out for distorted crystals by several authors (Klar & Rustichelli, 1973; Gronkowski & Malgrange, 1984; Kulda, 1984), but mainly by Kato (1976), who has partially reconciled the two approaches. He shows that for optical coherence lengths smaller than the extinction distance $\Lambda$ the new treatment leads to the usual coupling equations. Kato (1980) has also developed a consistent statistical theory of extinction covering the whole range of crystal quality from perfect (dynamical theory) to ideally imperfect (kinematical approximation). The results of this last theory have recently been compared to those of previous ones (Becker & Dunstetter, 1984) and experimentally tested using polarized neutrons (Guigay, Schlenker, Baruchel & Schweizer, unpublished).

0108-7673/86/010047-09$01.50 

A considerable theoretical effort, supported by a large amount of experimental evidence, was thus furnished to improve the extinction corrections in the neutron nuclear diffraction case. However, only a little has been published about the extinction in magnetic scattering, a pioneering paper being published by Hamilton in 1958. Nathans, Shull, Shirane & Andresen (1959) observed that the measured flipping ratios are more different from 1 when recorded on the flanks of the rocking curve and not, as is customary, at the maximum of the peak. This occurs when secondary extinction is present and was used, in an improved form, by Van Laar, Maniawski & Kaprzyk (1979) to measure accurately the structure factors on samples previously treated to remove primary extinction. Other treatments for the extinction when there is a mixture of both nuclear and magnetic scattering were given by Brown (1970) and, more recently, by Yelon, Van Laar, Kaprzyk & Maniawski (1984) for highly deformed specimens. As a general rule, the usual treatments were applied to magnetic diffraction just as they are, without considering the additional features associated with magnetic order. Indeed, the presence of crystal defects implies discontinuities in the magnetic structure and, in this way, gives rise to magnetic defects. The converse, however, may not be true since (1) the magnetic energies associated with the interactions of the magnetic moments are small relative to those between atoms in crystals, and (2) as the magnetic moments have directions, the imperfections in the magnetic structure can be associated with changes in this direction in addition to changes in the magnitude and position of the moments (Roth, 1970). A simple example, but far from being the only one, is a 180° wall. We will show, in this work, that failure to take these additional features into account in magnetic scattering can lead to very incorrect results in cases of severe extinction.

The present work was performed on the well studied MnP system, which crystallizes in the *Pbnm* orthorhombic space group ($a > b > c$). It can be grown as large high-purity low-mosaic-spread single crystals (Komatsubara, Kinoshita & Hirahara, 1965), resistivity ratios as high as 1300 having been obtained (Obara, Endoh, Ishikawa & Komatsubara, 1980) with mosaic spreads smaller than 1′. MnP is ferromagnetic below $T_c = 291$ K, **c** being the easy direction and **a** the hard one. It transforms into a helimagnetic phase at $T_s = 47$ K (Huber & Ridgley, 1964), the moments being arranged in ferromagnetic sheets in the *bc* plane, with **a** the helix axis. Felcher (1966) and Forsyth, Pickart & Brown (1966) have shown that the structure is actually a 'double spiral' (as shown in Fig. 1), with faint 'bunching' (Moon, 1982). A renewed interest in the material is partly associated with the search for a magnetic Lifshitz point (Shapira, Becerra, Oliveira & Chang, 1981).

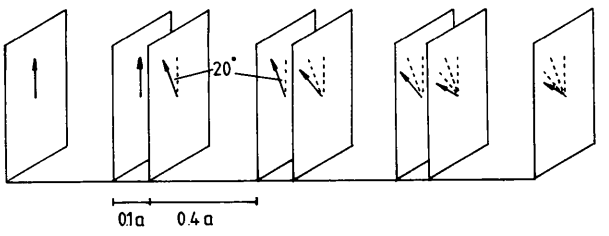


Fig. 1. Schematic diagram of the double spiral structure of MnP in its helimagnetic phase (after Felcher, 1966).

## II. Experimental results

The magnetic helical arrangement gives rise to neutron magnetic Bragg scattering in satellites located at points $\pm\tau$ from the reciprocal-lattice points *hkl* ($hkl_+$ and $hkl_-$ respectively), $\tau$ being the propagation vector of the helix. The magnetic scattering cross sections have different values in the case of MnP as the helix is not simple but double (Fig. 1). The sample investigated was a (100) platelet 0·93 cm$^2$ with a starting thickness of 0·11 cm. Another (100) sample 0·4 cm$^2$ by 0·05 cm was just measured for comparison. We concentrated on the 200 and $200_\pm$ reflections, *i.e.* all the diffraction experiments were performed in the symmetrical Bragg geometry situation. The experiments were carried out on the D13 diffractometer at ILL using a low-mosaic-spread (<1′) Ge 111 monochromator and the sample was cooled using a closed-circuit helium refrigerator.

The nuclear scattering cross section $|F_N|^2$ for the $200_N$ reflection is $6{\cdot}25\times10^{-28}$ m$^2$ and the average magnetic cross section for its satellites was found in the literature as $0{\cdot}58\times10^{-28}$ m$^2$ (Forsyth, Pickart & Brown, 1966) or $0{\cdot}32\times10^{-28}$ m$^2$ (Obara, Endoh, Ishikawa & Komatsubara, 1980). The ratio between the $200_-$ and $200_+$ cross sections is ~0·7. The expected ratio between the integrated reflectivities $I_+$ and $I_-$ over $I_N$ ($R_+$ and $R_-$) are thus ~0.1. Fig. 2 shows the experimental ratios measured on the sample at 20 K set with **c** vertical (before any surface treatment after spark machining). They are about ten times bigger

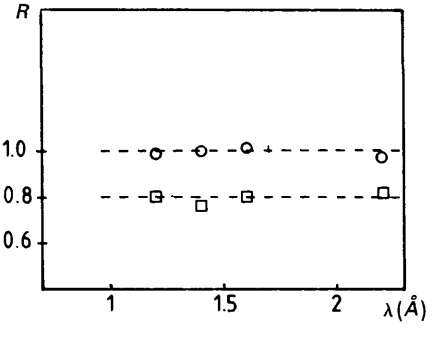


Fig. 2. The dependence of the ratios $R_+$ and $R_-$ on wavelength. ○ $R_+ = I_+/I_N$; □ $R_- = I_-/I_N$.

than expected and nearly constant with wavelength, indicating that this is not a multiple diffraction effect. When the sample was set with **b** vertical, they were reduced to ~0·87 and ~0·70, indicating anisotropic extinction, but were still constant with wavelength. The second sample, which was measured for comparison, gives the ratios as 0·44 and 0·38, still four times larger than expected. The 020 reflections, which are in the Laue geometry in our experiment, exhibit nuclear and magnetic scattering cross sections close to those of the 200 reflections. Similar effects, *i.e.* ratios $R_+$ and $R_-$ not far from 1, were observed when measuring the integrated reflectivities of these Bragg peaks. All these results indicate a strong extinction effect. We decided to investigate carefully the more severely extinguished case and the following results concern the first sample set with **c** vertical.

The sample thickness was reduced in stages by careful polishing with fine-grain emery paper followed by 6 μm diamond paste. Care was taken to maintain the surface state as constant as possible because, although this is not usually an important parameter in neutron work (Cooper & Walker, 1976), the nuclear intensity was observed to drop by a factor of 1·5 after the initial polish, the magnetic intensities remaining almost the same. Rocking curves of the 200 reflections were performed after each polish and the incident monochromatic beam ($\lambda = 2{\cdot}2$ Å, ~67 neutrons $mm^{-2}\,s^{-1}$) measured in order to obtain absolute reflectivities, corrections being made for cryostat absorption and geometrical factors. Scattering from the $200_-$ satellite occurs nearly in the $(+-)$ parallel setting at $\lambda = 1{\cdot}6$ Å; the width of this rocking curve, about 1·1′, indicates a very small sample mosaic spread (<1′).

Fig. 3 shows the results obtained at 20 K, in the helimagnetic phase, for the absolute reflectivities $\rho$ as a function of the effective thickness of the sample $t = t_0/\sin\theta$ ($\theta$ is slightly different for the various 200 reflections). The dotted lines are just guides for the eye. The nuclear reflectivity $\rho_N$ appears to be fairly constant over the whole range of investigated thickness $t$. The magnetic reflectivities $\rho_+$ and $\rho_-$ diminish regularly when the thickness is decreased, crossing the average $\rho_N$ at $t \sim 1{\cdot}2$ mm, and varying from about twice to less than half of this value. The scatter of the experimental points for the higher values of $t$ is not mainly due to counting statistics, but more probably to the many experimental difficulties like beam profile and constant sample preparation. This scatter does not affect a first, evident, conclusion that, in spite of their cross sections being ten times smaller than the nuclear cross section, the magnetic peaks can display reflecting powers bigger than the nuclear one. This implies that magnetic and nuclear extinction parameters behave in very different ways.

We measured the reflecting power $\rho_F$ of the 200 mixed nuclear+magnetic reflection in the ferromagnetic phase (Fig. 4). The measurements were not all recorded at exactly the same temperature, but were always in the range 70–100 K, where the magnitude of the magnetic moment is almost constant with temperature. The value of $\rho_F$, while bigger than the previously measured reflecting powers, is far from being their sum. It increases, over the whole range of investigated thickness, by a factor ~1·5, whereas $\rho_N$ is nearly constant and $\rho_+$ and $\rho_-$ are enhanced by a factor of ~4 over the same range.

### III. Which extinction models are possible?

The experimental results show a very unusual behaviour of the relative magnetic and nuclear reflecting powers, $\rho_\pm$ being bigger than $\rho_N$ when the sample is thick enough. An extinction model that assumes the same distortion for the nuclear and the magnetic cases [for instance, a curvature of the sample, as in Klar & Rustichelli (1973), or a gradient of the lattice parameter or a mosaic spread, like in Bacon & Lowde's (1948) paper] appears to be in contradiction

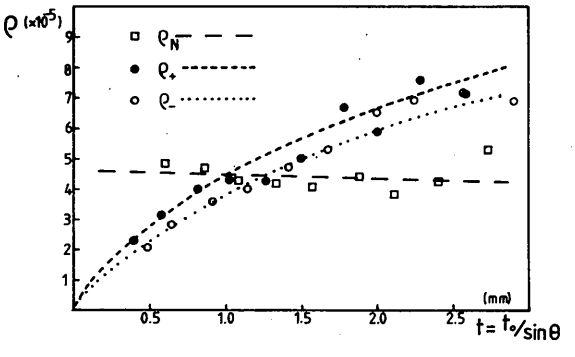


Fig. 3. The variation of the absolute reflectivities $\rho_+$, $\rho_-$ and $\rho_N$ of the $2 \pm \tau$, 0, 0 and $200_N$ reflections in the helimagnetic phase as a function of sample thickness. The dotted lines are just guides for the eye. $T = 20$ K; $\lambda = 2{\cdot}2$ Å.

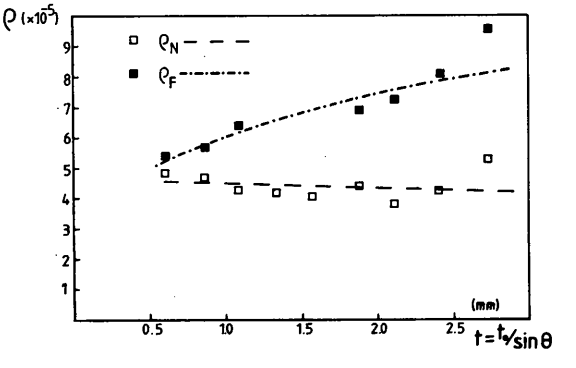


Fig. 4. The variation of the absolute reflectivity $\rho_F$ of the 200 reflection in the ferromagnetic phase as a function of the sample thickness. The values of $\rho_N$ in the helimagnetic phase are shown for comparison. The dotted lines are just guides for the eye. $\lambda = 2{\cdot}2$ Å.

with these experimental facts. Indeed, (1) the nuclear reflecting power does not increase with sample thickness, and (2) models of this kind can only predict a magnetic reflecting power nearly equal to the nuclear case, but not twice as big. This second point is supported by the following argument: the angular range of diffraction for the magnetic peak cannot exceed that of the nuclear peak if the distortion is the same, and the reflecting power for the individual plane-wave components cannot be expected to be bigger.

We are thus led to invoke a model involving either defects behaving, from the diffraction point of view, differently in the nuclear and magnetic cases, or defects purely magnetic in origin. We could imagine, for instance, that a dislocation or an inclusion could have an effective distorted region of larger extension around its core in the magnetic case than in the nuclear one. To the best of our knowledge this point has not been investigated. A simple model, based on the most common 'purely magnetic' defects, *i.e.* domain walls, with the assumption that the nuclear diffraction behavior is as for a perfect crystal, will be developed.

In the helimagnetic phase chirality domains, *i.e.* regions of the sample differentiated by the sense of rotation of the spiral, were observed on several MnP samples produced in the same laboratory as the one we are concerned with, using the technique of neutron diffraction topography (Patterson, Palmer, Baruchel & Ishikawa, 1985). They mainly appear as stripes lying normal to the helix axis in all the investigated cases.

No domains were thus observed topographically when investigating (100) platelets, because they are parallel to the surface (Fig. 5). Magnetostriction is believed to be the same for both kinds of domains; there is thus no variation of the distortion of the crystallographic lattice when going from one domain to the other, and their presence consequently do not modify the nuclear scattering. Magnetic scattering, on the other hand, is very sensitive to chirality domains. Indeed, the scattering cross section for a domain having a given chirality, and a given magnetic satellite $hkl_{\pm}$, is proportional to $[1+(\mathbf{e}\,.\,\mathbf{z})^2 \pm 2(\mathbf{p}\,.\,\mathbf{e})\times(\mathbf{z}\,.\,\mathbf{e})]$, where **e**, **z** and **p** are unit vectors along, respectively, the diffraction vector, the helix axis and the neutron polarization. The $\pm$ sign is reversed when considering the other chirality. The incident unpolarized neutron beam can be regarded as the addition of two neutron beams of equal intensity but opposite polarization along the quantization axis of our problem, *i.e.* the helix axis. The helix axis **a** and the diffraction vector are parallel in our experiment. In this situation the neutrons that are scattered by a given domain are completely different from those scattered by the following one because their polarizations are opposite and, therefore, there is no coherence at all between the beams diffracted by the two kinds of domain. Furthermore, the helix phase relationship is not expected to be conserved between one domain and the following one displaying the same chirality.

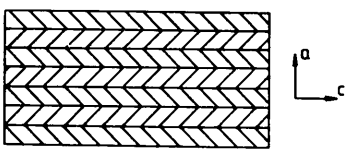


Fig. 5. Schematic diagram of the (heli- and ferro-) magnetic domain patterns in the investigated MnP sample.

In the ferromagnetic phase the only domain walls that are expected when taking into account the magnetically hard **a** axis are 180° walls lying in the (100) plane, as observed by Nagai, Hihara & Hirahara (1970). Thus, as in the helimagnetic phase, the probable domain pattern in the (100) plate consists of a series of stripes parallel to the surface (Fig. 5). Ferromagnetic walls and chirality domains are thought to be related: for a defect-free sample the width of the ferromagnetic walls should diverge when approaching the ferro-helimagnetic transition (Lajzerowicz & Niez, 1979). It can be easily deduced, from simple arguments, that the width of the chirality domains is, on average, twice that of the 180° ferromagnetic domains. Now, the magnetization lies along the magnetically easy **c** axis, which is the quantization axis in this phase. As before, the unpolarized incident beam can be considered as the addition of two beams polarized along the quantization axis. For a given neutron polarization the structure factors are, for the two domains, $F_+ = F_N + F_M$ and $F_- = F_N - F_M$. As none of these structure factors is zero (unlike in the helimagnetic phase), a fraction of the neutrons participate in the scattering in the two kinds of domains, and a partial coherence between the beams diffracted by the two kinds of domain is to be expected.

All these elements lead us to consider the model of the following section.

## IV. A possible model: nearly perfect crystal with type II secondary magnetic extinction

### (*A*) *Reflecting power in the helimagnetic phase*

The nuclear reflecting power $\rho_N$, not varying much with the crystal thickness, appears at least qualitatively similar to $\rho_{\rm dyn}$, the reflecting power of a perfect crystal in the Bragg case (Fig. 6) (Zachariasen, 1945)

$$\rho_{\rm dyn} = (\lambda^2|F|/V\sin 2\theta)\tanh(t_0/\Lambda) = \rho^{\infty}\tanh(t_0/\Lambda) \qquad (1a)$$

$$\Lambda = V\sin\theta/\lambda|F|, \qquad (1b)$$

where $\Lambda$ is the extinction period in the Bragg sym-

metrical setting ($V$ being the volume of the unit cell and the other symbols having their usual meanings).

The average of the experimental $\rho_N$ is $\sim 4{\cdot}4\times10^{-5}$, the value of $\rho_N^\infty$ for the 200 reflection of MnP being $1{\cdot}75\times10^{-5}$. The experimental value can be accounted for by assuming (1) that the bulk of the sample behaves as a nearly perfect crystal, *i.e.* that its contribution is $\rho_N^\infty$, since the thickness of the crystal is always much bigger than $\Lambda_N$ ($\sim 7$ μm) (see Fig. 6), and (2) that the two surfaces, distorted by the polishing, can be described by two layers behaving in a kinematical way over an 'effective distorted distance' $2d_0$. The value of $d_0$ should be of the same order of magnitude as that of the diamond grain diameter ($\sim 6$ μm). Absorption is not completely negligible and is taken into account when considering the intensity diffracted by the back surface. The experiments having been performed at low temperatures, TDS and Debye-Waller corrections were assumed negligible throughout this work.

The total reflecting power per unit surface is thus

$$\rho_N = \rho_N^\infty + Q_N d(1+e^{-2\mu t}), \qquad (2a)$$

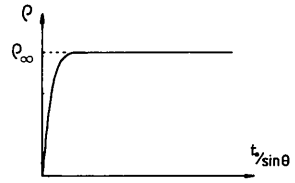


Fig. 6. The reflectivity of a perfect crystal from dynamical theory in the Bragg case as a function of thickness. The saturation value $\rho_{dyn}^\infty$ is reached for a sample thickness of approximately 2 $\Lambda$.

where

$$Q_N = |F_N|^2\lambda^3/V^2\sin 2\theta_N \quad \text{and} \quad d = d_0/\sin\theta_N. \qquad (2b)$$

We need to take $d_0 = 5{\cdot}3$ μm (which is physically reasonable) to fit the experimental results (Fig. 7*a*).

It appears less straightforward to explain the behaviour of the two magnetically scattered curves. The reflecting power per unit surface $\rho$ of a platelet can always be compared with the kinematical reflecting power $\rho_{kin}$, and described by the relation

$$\rho = \rho_{kin} y = Q[(1-e^{-\mu t})/\mu]y, \qquad (3)$$

where $t = t_0/\sin\theta$ is the thickness of the platelet along the neutron beam, $[(1-e^{-\mu t})/\mu]$ is an effective thickness that takes the absorption into account (Zachariasen, 1967) and $y$ is the extinction parameter.

We saw in the previous section that the sample is composed, from the magnetic diffraction point of view, of thin optically independent slices (the chirality domains) parallel to the surface, with no misorientation between neighbouring slices. For the particular reflections we are concerned with such a crystal is similar to the model defined by Zachariasen as type II secondary extinction (as opposed to type I, where extinction is dominated by the misorientation between mosaic blocks). In the type II model the natural width of the reflection from a single block is greater than the mosaic-spread parameter. The extinction is thus mainly due to the size of the blocks, which gives rise to an apparent mosaic spread $\sim\lambda/r$. Zachariasen (1967) worked out a very simple and

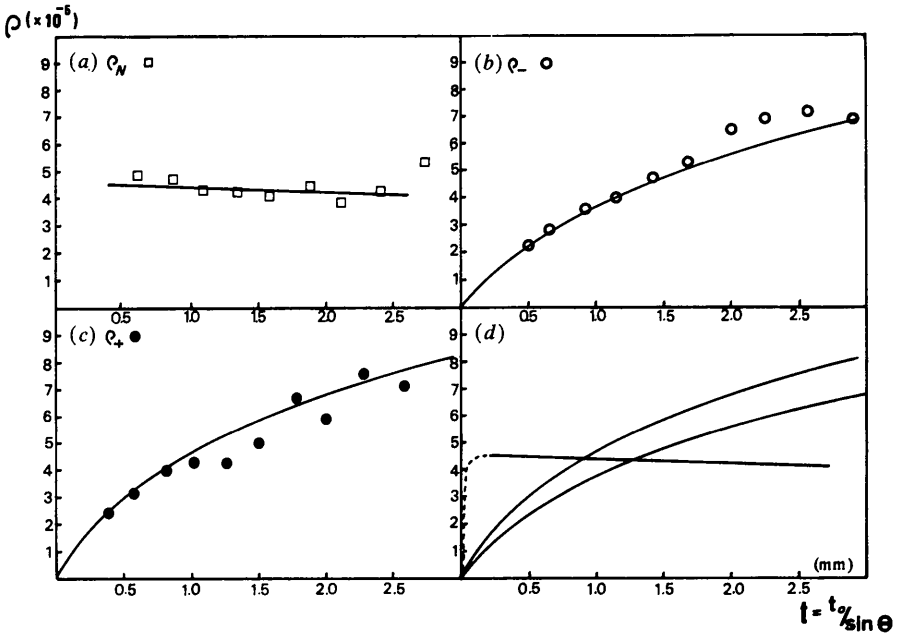


Fig. 7. The experimental points and calculated curves for (*a*) $200_N$, (*b*) $2-\tau, 0, 0$, (*c*) $2+\tau, 0, 0$ in the helimagnetic phase; (*d*) whole set of calculated curves on the same graph. ($T = 20$ K, $\lambda = 2{\cdot}2$ Å.)

commonly used expression for the extinction parameter $y$,

$$y = (1+2\bar{x}_0)^{-1/2} \tag{4a}$$

with

$$\bar{x}_0 = \lambda^{-1} r Q t \sin 2\theta, \tag{4b}$$

in the type II approximation, which requires $r \ll \Lambda$. (This excludes the simultaneous presence of type II secondary extinction and of primary extinction.) The angular dependence has been introduced in $\bar{x}_0$ following Becker & Coppens (1974*a*).

The expression $r \sin 2\theta$ in (4*b*), $r$ being the spherical radius, should be substituted in our case by $(4r_0 \cos\theta)/3$, with $r_0$ the average thickness of the chirality domains.

It is possible to obtain experimental values for $Q_+$ and $Q_-$ (and thus for the cross sections $|F_+|^2$ and $|F_-|^2$) by extrapolating the experimental curves to $t=0$ and measuring the slopes of the tangents at this point. We preferred to employ this self-consistent procedure instead of using calculated values for $Q$, based on published data, in spite of its poor accuracy. We find $Q_+ = 9{\cdot}3(7)$ and $Q_- = 6.8(6)\ \mu m^{-1}$, which correspond to average values $|F_+|^2 = 0{\cdot}62 \times 10^{-28}\ m^2$ and $|F_-|^2 = 0{\cdot}41 \times 10^{-28}\ m^2$. These last values are intermediate between those found in the literature and close to those published by Forsyth, Pickart & Brown (1966).

Figs. 7(*b*) and (*c*) show the experimental points and the curves calculated using the above values for $Q_\pm$ and taking $r_0 = 2{\cdot}8\ \mu m$. The distorted regions near the surface have not been taken into account because their contribution to scattering here is very weak, as indicated by the experimental fact that the initial polish, whereas reducing significantly the nuclear intensity, has no effect on the magnetic ones. Fig. 7(*d*) shows the whole set of calculated curves together.

### (*B*) *Reflecting power in the ferromagnetic phase*

The results for the ferromagnetic phase will be treated in a similar manner to those of the helimagnetic one. As pointed out before, a partial coherence is expected between neutrons scattered from both types of domain in this phase. A factor $\alpha$ is introduced to allow, in a phenomenological way, for this partial coherence of the diffraction. The whole incoming neutron beam is scattered in a kinematical way by the distorted surfaces, but only a fraction $(1-\alpha)$ of the neutrons 'see' the crystal as being uniform all through their path within the sample, the rest of them (fraction $\alpha$) being diffracted as for a crystal composed by several optically incoherent blocks. The reflecting power $\rho_F$ contains in the present crude approximation three terms:

$$\rho_F = (1-\alpha)\rho^{\infty}_{dyn} + Q_F d(1+e^{-2\mu t}) + \alpha Q_F[(1-e^{-\mu t})/\mu]y, \tag{5}$$

these being (1) the perfect-crystal-like bulk scattering, (2) the kinematical scattering from the distorted surfaces, and (3) the type II secondary-extinction bulk scattering, respectively. In the first term $\rho^{\infty}_{dyn}$ results from the addition of the dynamical diffraction for both polarizations, with structure factors $F_+$ and $F_-$, and its value is thus just equal to $\rho^{\infty}_N$. A scattering cross section $|F_F|^2 = |F_N|^2 + |F_M|^2$ is used for the other two terms. In the second term the effective width $d$, which describes the scattering by the surfaces, should be of the same order as for the spiral phase, but slightly smaller owing to a slight increase in the scattering cross section.

The average width of the domains in the ferromagnetic phase should be half that in the helimagnetic phase. The chirality domain width was described, in the extinction formalism, by $r_0 = 2{\cdot}8\ \mu m$. It appears sensible then to take $r_0 = 1{\cdot}4\ \mu m$ in the present case.

The fit shown in Fig. 8 was obtained from (5) using values of $\alpha = 0{\cdot}12$ and $d_0 = 4\ \mu m$, which are not physically unreasonable. Fig. 8 also shows how the calculated $\rho_F$ is situated with respect to the average $\rho_N$ measured in the helimagnetic phase. The physical meaning of these results will be discussed in § VI.

## V. Reflectivity ratios $R_+$ and $R_-$ as a function of wavelength

A tentative explanation of the results of Fig. 2, *i.e.* the invariance of $R_\pm$ with wavelength, can be deduced from our general arguments about the reflecting power as a function of the neutron wavelength. The reflectivity of a perfect crystal in the symmetrical Bragg case given in (1) can be rewritten as

$$\rho_{dyn} = (d_h/t_0)(\tan\theta) A \tanh A, \tag{6}$$

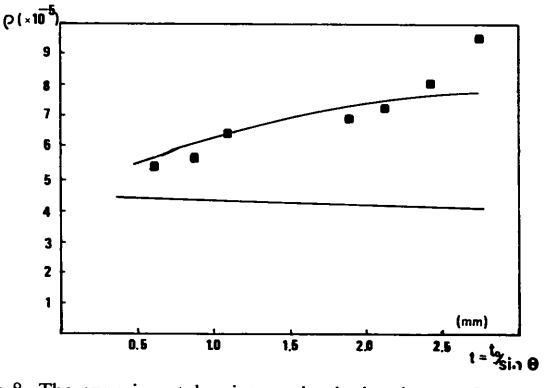


Fig. 8. The experimental points and calculated curve for the 200 reflection in the ferromagnetic phase. The calculated curve for the $200_N$ reflection in the helimagnetic phase (dotted line) is shown for comparison ($\lambda = 2{\cdot}2$ Å).

in which $d_h$ is the distance between successive reflecting planes and $A$ is a reduced parameter:

$$A = t_0/\Lambda = 2(d_h F t_0)/V. \quad (7)$$

The ideally imperfect crystal case is obtained as the limit of $\rho_{dyn}$ for $A \to 0$:

$$\rho_{kin} = (d_h/t_0)(\tan\theta)A^2. \quad (8)$$

This formulation suggests that, at least in some cases, the real crystal case could be described by replacing $A \tan A$ or $A^2$ by some unknown function of the same parameter $A$. If this is true, $\rho/\tan\theta$ would be independent of $\lambda$. The ratios of the easily measured quantities

$$i_\pm = I_\pm/\tan\theta_\pm \quad \text{and} \quad i_N = I_N/\tan\theta_N$$

would consequently be independent of $\lambda$ (it is experimentally simpler to consider intensity ratios in order to eliminate the incident intensity). This idea is in good agreement with our measurements of $R_\pm$ shown in Fig. 2. (The angular factor is practically constant for the range of wavelength we are concerned with.)

## VI. Discussion

Fig. 9 shows the 'experimental' extinction parameter $y$, obtained by dividing the measured reflecting power by the kinematical value just corrected for absorption.

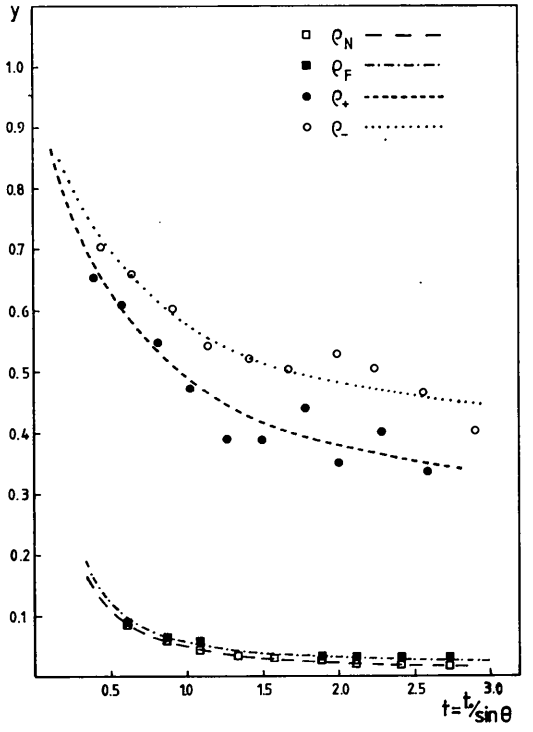


Fig. 9. The experimental value of the extinction parameter $y$ as a function of the sample thickness for the whole set of 200 reflections. The dotted lines are just guides for the eye.

It can be observed that all the values of $y$ are smaller than 0·7, some of them being as small as $2{\cdot}5 \times 10^{-2}$. These very severe extinction effects are beyond those usually observed and corrected for by extinction models.

We are, nevertheless, able to account for these results, in a phenomenological way, by using a 'perfect' crystal and/or Zachariasen's type II secondary extinction theories. It was pointed out by several authors (Becker & Coppens, 1974*a*, *b*; Cooper & Rouse, 1976) that the simple expression (4) leads to satisfactory results only for $y > 0{\cdot}7$, just out of the range of the present work (Fig. 9). The physical meaning of the values we derived for the various parameters, which is always a non-trivial problem, appears thus to be even more difficult in our case. Some comparisons of block sizes, $r$, with dislocation densities (Killean, Lawrence & Sharma, 1972; Sharma, 1974) seem to indicate that Zachariasen's theory leads to physically unrealistic results. However, Becker & Coppens (1974*b*), when treating the same experimental results with their formalism, and taking into account the primary nature of extinction, concluded that the block size is in reasonable agreement with the dislocation density. The same conclusion is also reached by Olekhnovich, Markovich & Olekhnovich (1980). It has been pointed out by Nelmes (1980) that the essential purpose of extinction models is to describe adequately the difference between observed and calculated integrated intensities. Once this is achieved, the same model does not necessarily provide an accurate description of the actual microstructure of the crystal.

The values of $r_0$ obtained in this experiment are coherent with the initial assumption of the model ($r_0 \ll \Lambda$). In the helimagnetic case this value does not appear to be in agreement with the average size of chirality domains (0·1 mm) observed on several samples of various orientations (Patterson, Palmer, Baruchel & Ishikawa, 1985). For the model to work there must be a loss of coherence between blocks. Three possibilities can be conceived when maintaining the assumption that the form (4*a*) of the extinction parameter $y$ is the adequate one: (1) that in this sample the chirality domains have an average size of 2·8 μm; (2) that these domains are 0·1 mm in size but there is a loss of coherence along the spiral every 2·8 μm without reversing the sense of chirality; and (3) that the actual physical domains of unknown thickness (maybe 0·1 mm) are described in an effective way in this extinction formalism by blocks of 2·8 μm. The first and third points should also hold for the ferromagnetic case, but the second one, having no ferromagnetic counterpart, is more difficult to admit. Another possibility could be, of course, to try to apply more elaborate theories of extinction (Werner, 1974; Kato, 1980).

**Summary**

One of the most striking experimental effects observed is that two magnetic satellites having scattering cross sections ten times smaller than the nuclear reflection have reflectivities nearly twice as great as the nuclear case. The purely nuclear scattering data can be described from dynamical theory but another approach is needed to describe the magnetic effects. We used a model based on secondary extinction, which starts from the chirality domain structure of the sample. The explanation we give for the ferromagnetic data integrates elements of the two approaches, the ferromagnetic domains replacing, with half the width, the chirality domains. It is interesting to note that in our case the mixed nuclear + magnetic reflection is less extinguished than the corresponding nuclear one. If domains are at the root of the problem then, in the ferromagnetic case, they can be removed by applying a magnetic field (which would increase the extinction) but we do not know of any method of obtaining a single-domain helimagnet. The invariance of the $R_{\pm}$ ratios with wavelength appears to be related to general diffraction arguments.

This work may appear marginal because, whereas it treats quite spectacular experimental facts, it deals with the diffraction of neutrons by nearly perfect - or at least very severely extinguished - magnetic crystals. This subject, covered theoretically by several works in the last years (Guigay, Schlenker & Baruchel, 1984, and references therein) is experimentally still new because only very few magnetic materials exhibiting a very high crystalline quality have been grown and therefore investigated. To the best of our knowledge, the only material studied by neutron diffraction from this point of view, excluding papers where severe extinctions were corrected for but where no emphasis was put on this problem (for instance, Shirane, Chikazume, Akimitsu, Chiba, Matsu & Fujii, 1975), is yttrium iron garnet (YIG) (Bonnet, Delapalme, Fuess & Becker, 1979; Baruchel, Guigay, Mazuré-Espejo, Schlenker & Schweizer, 1982).

The present work presents one possible model, but other models based on the different effective width of defects when viewed by magnetic and nuclear reflections or on more rigorous treatments of extinction appear to be possible. The main point to be emphasized here is the experimentally observed different extinction effects for magnetic and nuclear reflections when separated peaks exist (antiferromagnetic-type materials).

These differences were encountered, in an attenuated form, in a range of magnetic materials far larger than nearly perfect crystals (on $MnF_2$ or on pure Tb and Ho crystals, for instance). The reason this kind of phenomena does not appear in the literature could just be because the results were not explained in a satisfactory way for the authors. With the increased availability of good-quality magnetic single crystals, great progress could be made in this field allowing experimental verification of the more curious aspects of dynamical magnetic theory.

The authors express their gratitude to Professor Y. Ishikawa for the provision of the MnP samples, valuable discussions and his interest throughout this work, and to Professor P. Becker for very useful remarks.

**References**

BACON, G. E. & LOWDE, R. D. (1948). *Acta Cryst.* **1**, 303-314.
BARUCHEL, J., GUIGAY, J. P., MAZURÉ-ESPEJO, C., SCHLENKER, M. & SCHWEIZER, J. (1982). *J. Phys. (Paris)*, **12**, C7, 101-106.
BECKER, P. & COPPENS, P. (1974*a*). *Acta Cryst.* **A30**, 129-147.
BECKER, P. & COPPENS, P. (1974*b*). *Acta Cryst.* **A30**, 148-153.
BECKER, P. & COPPENS, P. (1975). *Acta Cryst.* **A31**, 417-425.
BECKER, P. & DUNSTETTER, F. (1984). *Acta Cryst.* **A40**, 241-251.
BONNET, M., DELAPALME, A., FUESS, H. & BECKER, P. (1979). *J. Phys. Chem. Solids*, **40**, 863-876.
BROWN, P. J. (1970). In *Thermal Neutron Diffraction*, edited by B. T. M. WILLIS, pp. 176-189. Oxford Univ. Press.
COOPER, M. J. & ROUSE, K. D. (1970). *Acta Cryst.* **A26**, 214-223.
COOPER, M. J. & ROUSE, K. D. (1976). *Acta Cryst.* **A32**, 806-812.
COOPER, M. J. & WALKER, C. R. (1976). *Acta Cryst.* **A32**, 813-815.
COPPENS, P. & HAMILTON, W. C. (1970). *Acta Cryst.* **A26**, 71-83.
FELCHER, G. P. (1966). *J. Appl. Phys.* **37**, 1056-1058.
FORSYTH, J. B., PICKART, S. J. & BROWN, P. J. (1966). *Proc. Phys. Soc. London*, **88**, 333-339.
GRONKOWSKI, J. & MALGRANGE, C. (1984). *Acta Cryst.* **A40**, 507-514, 515-522.
GUIGAY, J. P., SCHLENKER, M. & BARUCHEL, J. (1984). In *Application of X-ray Topographic Methods to Materials Science*, Edited by S. WEISSMANN, F. BALIBAR & J. F. PETROFF, pp. 171-182. New York: Plenum Press.
HAMILTON, W. C. (1958). *Acta Cryst.* **11**, 585-593.
HUBER, E. E. & RIDGLEY, D. H. (1964). *Phys. Rev. A*, **135**, 1033-1040.
KATO, N. (1976). *Acta Cryst.* **A32**, 453-457.
KATO, N. (1980). *Acta Cryst.* **A36**, 763-769, 770-778.
KILLEAN, R. C. G., LAWRENCE, J. L. & SHARMA, V. C. (1972). *Acta Cryst.* **A28**, 405-407.
KLAR, B. & RUSTICHELLI, F. (1973). *Nuovo Cimento B*, **13**, 249-271.
KOMATSUBARA, T., KINOSHITA, K. & HIRAHARA, E. (1965). *J. Phys. Soc. Jpn*, **20**, 2036-2045.
KULDA, J. (1984). *Acta Cryst.* **A40**, 120-126.
LAJZEROWICZ, J. & NIEZ, J. J. (1979). *J. Phys. Lett.* pp. L-165-169.
MOON, R. M. (1982). *J. Appl. Phys.* **53**, 1956-1957.
NAGAI, H., HIHARA, T. & HIRAHARA, E. (1970). *J. Phys. Soc. Jpn*, **29**, 622-632.
NATHANS, R., SHULL, C. G., SHIRANE, G. & ANDRESEN, A. (1959). *J. Phys. Chem. Solids*, **10**, 138-146.
NELMES, R. J. (1980). *Acta Cryst.* **A36**, 641-653.
OBARA, H., ENDOH, Y., ISHIKAWA, Y. & KOMATSUBARA, T. (1980). *J. Phys. Soc. Jpn*, **49**, 928-935.
OLEKHNOVICH, N. M., MARKOVICH, V. L. & OLEKHNOVICH, A. I. (1980). *Acta Cryst.* **A36**, 989-996.
PATTERSON, C., PALMER, S. B., BARUCHEL, J. & ISHIKAWA, Y. (1985). *Solid State Commun.* **55**, 81-84.
ROTH, W. L. (1970). In *The Chemistry of Extended Defects in Non-Metallic Solids*, pp. 455-487. Amsterdam: North-Holland.
SHAPIRA, Y., BECERRA, C. C., OLIVEIRA, N. F. & CHANG, T. S. (1981). *Phys. Rev. B*, **24**, 2780-2806.

SHARMA, V. C. (1974). *Acta Cryst.* A30, 278-280.
SHIRANE, G., CHIKAZUMI, S., AKIMITSU, J., CHIBA, K., MATSU, M. & FUJII, Y. (1975). *J. Phys. Soc. Jpn*, **39**, 949-957.
THORNLEY, F. R. & NELMES, R. J. (1974). *Acta Cryst.* A30, 748-757.
VAN LAAR, B., MANIAWSKI, F. & KAPRZYK, S. (1979). *Acta Cryst.* A35, 468-475.
WERNER, S. A. (1969). *Acta Cryst.* A25, 639.
WERNER, S. A. (1974). *J. Appl. Phys.* **45**, 3246-3254.
YELON, W. B., VAN LAAR, B., KAPRZYK, S. & MANIAWSKI, F. (1984). *Acta Cryst.* A40, 16-23.
ZACHARIASEN, W. H. (1945). *Theory of X-ray Diffraction in Crystals.* New York: Dover.
ZACHARIASEN, W. H. (1967). *Acta Cryst.* **23**, 558-564.

*Acta Cryst.* (1986). A42, 55-56

# Two-Dimensional Space Groups with Sevenfold Symmetry

BY ALAN L. MACKAY

*Department of Crystallography, Birkbeck College (University of London), Malet Street, London WC1E 7HX, England*

(*Received* 16 *April* 1985; *accepted* 22 *August* 1985)

## Abstract

Fivefold and sevenfold symmetry operations are, of course, incompatible with repetition by a lattice but, with the appearance of structures involving curved sheets, they and other non-crystallographic operations must now be taken into consideration as possibilities of non-Euclidean crystallography develop. Here are described the symmetry groups which might be called 732 and $73m$ and which may be found in two-dimensional manifolds.

Structures with fivefold symmetry on the surface of a sphere have been familiar at least since the work of Caspar & Klug (1962). There are two ways of regarding the packing of units on the surface of a sphere:

(*a*) they may be considered as forming a finite particle with the three-dimensional point symmetry groups 532 or $53m$ for which there are respectively (depending on whether mirror symmetry is forbidden or permitted) 60 and 120 fundamental regions or asymmetric units of pattern; or

(*b*) they may be considered as a packing in two-dimensional curved space of non-Euclidean metric. This approach enables us to bring sevenfold (and higher) symmetry within the compass of crystallography.

The curvature arises because five units, which may be equilateral triangles, pack around a fivefold axis to give an icosahedron. If the edges of this icosahedron are projected radially on to the circumscribed sphere then a tessellation of spherical triangles is obtained. The sum of the angles of a triangle made up of geodesics on the surface is given by

$$\alpha+\beta+\gamma=\pi+\int K\,\mathrm{d}S,$$

where $K$ is the Gaussian curvature of the surface. As the curvature is positive the surface closes on itself and is of finite area.

At any point in a surface there will be two principal curvatures $K_1$ and $K_2$ in perpendicular planes. The mean (or first) curvature is $J=(K_1+K_2)/2$ and the Gaussian (or second) curvature is $K=K_1K_2$.

In any extended plane tessellation of triangles, the mean coordination number of a point is six. If the coordination number is less than six then a spherical or positively curved elliptical space is obtained. However, if the mean coordination number is greater than six a curved two-dimensional space is obtained having hyperbolic or negative Gaussian curvature. A graphic illustration of a surface where the local coordination in the surface is greater than six is provided by a frond of crinkled seaweed such as *Fucus letuca*, where the area out to a distance $r$ from any given point increases faster than $\pi r^2$. In fact, the circumference of a small circle on a surface of Gaussian curvature $K$ is given by $s(r)=2\pi r-(1/3)\pi Kr^3+$terms in $r^5$ and higher powers. If the space is curved and non-Euclidean then the parallel postulate of Euclid fails and the concept of repetition on a lattice must be abandoned. On the surface of a sphere the asymmetric units are repeated by rotations and reflections. In addition to the groups 532 and $53m$, the axial groups $N$, $N2$, $N/m$ are well known.

The surface of a sphere is, of course, a finite space but surfaces with negative Gaussian curvature may be infinite. Some of these have recently come into

0108-7673/86/010055-02$01.50